Axion Constraints from Quiescent Soft Gamma-ray Emission from Magnetars

Sheridan J. Lloyd,[a)] Paula M. Chadwick,[b)] and Anthony M. Brown[c)]
Centre for Advanced Instrumentation, Dept. of Physics, University of Durham, South Road, Durham, DH1 3LE, UK

Huai-ke Guo[d)] and Kuver Sinha[e)]
Department of Physics and Astronomy, University of Oklahoma, Norman, OK 73019, USA

Axion-like-particles (ALPs) emitted from the core of magnetars can convert to photons in the strong magnetic field of the magnetosphere. We study such emissions in the soft gamma-ray range from 300 keV to 1 MeV, where the ALP spectrum peaks and astrophysical backgrounds from resonant Compton upscattering are expected to be suppressed. Using published quiescent soft-gamma flux upper limits in 6 Magnetars obtained with *CGRO* COMPTEL, *INTEGRAL* SPI/IBIS/ISGRI and the *Fermi* Gamma Ray Burst Monitor (GBM), we put limits on the ALP-photon coupling obtained from conversions, assuming that ALP emission from the core is just sub-dominant to bounds from neutrino cooling. For core temperatures of 10^9 K, the constraints on the ALP-photon coupling coming from magnetars 1E 2259+586 and J170849.0-400910 are better than the current limits obtained from the CAST experiment. We provide a detailed study of the dependence of our results on the magnetar core temperature. Our results motivate a program of studying quiescent soft gamma ray emission from magnetars in the 300 keV - 1 MeV band with the *Fermi*-GBM.

Keywords: astroparticle physics – axion: general – gamma-rays: general – pulsars: general

I. INTRODUCTION

The axion arises in the context of a solution to the strong CP problem of QCD and is a plausible cold dark matter candidate [1–3]. The search for axions, and more generally axion-like-particles (ALPs) (for which the relationship between particle mass and the Peccei-Quinn scale is relaxed), now spans a vast ecosystem ranging from helioscopes, haloscopes, interferometers, beam dumps, fixed target experiments, and colliders. We refer to [4] for a review of this growing literature.

Our interest in this paper will be centered on the question of indirect detection of ALPs, specifically their conversion into photons in the magnetospheres of neutron stars with strong magnetic fields (magnetars) [5–7]. The mechanism is as follows[8]: relativistic ALPs (a) emitted from the core by nucleon (N) bremsstrahlung (from the Lagrangian term $\mathcal{L} \supset g_{aN}(\partial_\mu a)\bar{N}\gamma^\mu\gamma_5 N$) escape into the magnetosphere, where they convert to photons (from the Lagrangian term $\mathcal{L} \supset -\frac{1}{4}g_{a\gamma\gamma}aF_{\mu\nu}\tilde{F}^{\mu\nu}$) in the presence of the neutron star magnetic field B. The ALP emission rate has a very strong dependence on core temperature to the sixth power [9 and 10] while the conversion rate increases with stronger B, making magnetars, with their high core temperatures of $\sim 10^9$ K and strong magnetic fields $\sim 10^{14}$ G, a natural target for these studies.

The purpose of this paper is to initiate an investigation of the signals resulting from ALP-photon conversions in the quiescent soft-gamma ray spectrum (300 keV - 1 MeV) emanating from magnetars. Such signals have been probed in the soft and hard X-ray spectrum in previous work by one of the authors [5 and 6]. Since the peak of photon energies arising from ALP-photon conversion lies in the soft gamma ray band, this is an especially important regime to explore. Moreover, while searches for new physics in the soft and hard X-ray emission from magnetars must contend with background from thermal emission and resonant Compton upscattering respectively, the astrophysical background in the soft gamma-ray regime is relatively suppressed, as we shall discuss in detail.

Starting with the photon polarization tensor, we provide expressions for the photon refractive indices in the strong and weak magnetic field regimes for photon energies $\omega \lesssim 2m_e$, where m_e is the electron mass[11]. The coupled ALP-photon propagation equations are then solved numerically using the appropriate refractive indices. Assuming that g_{aN} is such that ALP production from nucleon bremsstrahlung in the core is just sub-dominant to neutrino production by modified URCA processes, we calculate the photon luminosity coming from ALP conversions and constrain $g_{a\gamma\gamma}$ by requiring that this luminosity be less than the observed soft gamma-ray flux. The calculations are performed for a selection of 6 magnetars using published quiescent soft-gamma flux upper limits obtained with *CGRO* COMPTEL, *INTEGRAL* SPI/IBIS/ISGRI and the *Fermi* Gamma Ray Burst Monitor (GBM). For two magnetars, 1RXS J170849.0-400910 and 1E 2259+586, the limits on the ALP-photon coupling $g_{a\gamma\gamma}$ beat the current limits from the CERN Axion Solar Telescope (CAST) for ALP masses $m_a \lesssim 10^{-4}$ eV, assuming a core temperature of 10^9K. We also study the robustness of our results as the core temperature is varied.

The main message of our paper is the following: quiescent soft gamma-ray emission from magnetars is a fertile target to investigate the physics of ALPs. The *Fermi*-GBM is a very useful instrument to determine the upper limit (UL) soft gamma-ray fluxes of the 23 confirmed magnetars from the McGill magnetar Catalog. A study of these magnetars by *Fermi*-GBM could yield very restrictive constraints on the ALP-photon coupling.

Before proceeding, we briefly place our paper in the context of prior work on ALPs and magnetars. In [12], cooling simulations, combined with surface temperature measurements of 4 thermal X-ray emitting pulsars (PSRs), have been used to determine $m_a < (0.06\text{-}0.12\text{ eV})$ for the QCD axion. In the gamma-ray regime, the authors of [13] have used 5 years of PASS 7 *Fermi*-LAT gamma-ray observations of radiative axion decay in 4 nearby PSRs to constrain $m_a < 0.079$ eV for the QCD axion, albeit reliant on very high pulsar core temperatures [7] to enhance the production rate appreciably. In contrast to cooling or decay, our work relies on *conversions* from ALPs to photons in the magnetosphere; moreover, we take a benchmark core temperature of 10^9K.

This paper is structured as follows. In Section II we discuss the phenomenology of ALP-photon conversions and compute the predicted emission. The details of the calculation of the predicted luminosity and the photon refractive index are contained in two appendices. In Section III we list our magnetar selection and previously obtained soft gamma determinations obtained by *INTE-GRAL*, the Compton Gamma Ray Observatory (*CGRO*) and the *Fermi* satellite. In Section IV we discuss the astrophysical background stemming from resonant Compton upscattering, whilst in V we consider the range of possible core temperatures for the magnetars in our sample. In Section VI we present our main results: the bounds on the ALP-photon coupling are shown in Figure 1, while the dependence of our results on the core temperature are shown in Figure 2 and Figure 3. In Section VII we discuss how the GBM could be used to make further magnetar observations in the soft gamma-ray band. Finally in Section VIII we summarise our findings and make suggestions for future work.

II. PHENOMENOLOGY

In this section, we discuss the predicted luminosity from ALP-photon conversion in the magnetosphere. We assume a dipolar magnetic field defined by

$$B = B_{surf}\left(\frac{r_0}{r}\right)^3 . \tag{1}$$

ALPs propagating radially outwards from a magnetar obey the following evolution equations derived in [14]

$$i\frac{d}{dx}\begin{pmatrix} a \\ E_\parallel \\ E_\perp \end{pmatrix} = \begin{pmatrix} \omega r_0 + \Delta_a r_0 & \Delta_M r_0 & 0 \\ \Delta_M r_0 & \omega r_0 + \Delta_\parallel r_0 & 0 \\ 0 & 0 & \omega r_0 + \Delta_\perp r_0 \end{pmatrix}\begin{pmatrix} a \\ E_\parallel \\ E_\perp \end{pmatrix}, \qquad \text{where} \tag{2}$$

$$\Delta_a = -\frac{m_a^2}{2\omega}, \qquad \Delta_\parallel = (n_\parallel - 1)\omega, \qquad \Delta_\perp = (n_\perp - 1)\omega, \qquad \Delta_M = \frac{1}{2}g_{a\gamma\gamma}B\sin\theta. \tag{3}$$

We note that the parallel and perpendicular electric fields are denoted by $E_\parallel(x)$ and $E_\perp(x)$, respectively, while $a(x)$ denotes the ALP field. The distance from the magnetar is given by the rescaled dimensionless parameter $x = r/r_0$, where r is the distance from the magnetar and r_0 its radius. The energy of the photon is given by ω, the ALP mass by m_a, and the ALP-photon coupling by $g_{a\gamma\gamma}$. The angle made by the direction of propagation with respect to the external magnetic field is given by θ.

The refractive indices $n_\parallel$ and $n_\perp$ are obtained from the photon polarization tensor, which can be worked out at one-loop level in various limits of the photon energy ω and the strength of the magnetic field B relative to the quantum critical magnetic field B_c. The critical magnetic field is given by $B_c = m_e^2/e = 4.413 \times 10^{13}$ G. Here $e = \sqrt{4\pi\alpha}$ and the fine structure constant is given by $\alpha \approx 1/137$.

Near the surface, the magnetic field of the magnetars we consider typically exceeds the quantum critical value.

We are thus in the regime $\omega \lesssim 2m_e$ and $B > B_c$. The corresponding refractive indices are given in Eq. B15. Given the spatial dependence from Eq. 1, the magnetic field decreases to below the critical strength at a distance $\sim 3r_0$. Beyond that, we are in a regime where $\omega \lesssim 2m_e$ and $B \ll B_c$, with $\left(\frac{\omega}{2m_e}\right)^2\left(\frac{B}{B_c}\right)^2 \ll 1$. The corresponding refractive indices are given in Eq. B14. We provide further details in Appendix B.

After calculating the parallel refractive index $n_\parallel$, the probability of conversion can be obtained as a function of the ALP-photon mixing $g_{a\gamma\gamma}$ and the mass m_a by numerically solving Eq. 2. The interesting regime for conversion turns out to be $r = r_{a\to\gamma} \sim \mathcal{O}(1000)\,r_0$ (the "radius of conversion), where the conversion probability becomes large. This can be understood from the fact that the ALP-photon mixing becomes maximal when $\Delta_M \sim \Delta_\parallel$. Far away from the surface, $\Delta_M \sim 1/r^3$, while $\Delta_\parallel \sim 1/r^6$ from Eq. B14, with the two becoming equal around $r_{a\to\gamma}$.

Along with the probability of conversion, we require the normalized ALP spectrum and the number of ALPs being produced from the core of the magnetar. Integrating the product of these quantities over the ALP energy range $\omega \subset (\omega_i, \omega_f) = (300\,\mathrm{keV}, 1000\,\mathrm{keV})$ gives us the final predicted luminosity from ALP-photon conversions. Our master equation for the final predicted photon luminosity is Eq. A3, which we solve numerically. A semi-analytic calculation following [6] is also performed to validate our results. We provide further details in Appendix A.

III. MAGNETAR SELECTION AND UL SOFT GAMMA-RAY FLUX DETECTION

We select 6 magnetars which have published ULs for differential energy fluxes in the soft gamma-ray band 300 keV to 1 MeV (Table I). The UL fluxes are obtained from the *INTEGRAL* Soft Gamma-Ray imager (ISGRI) detector, on the angular resolution Image on Board instrument (IBIS) and *INTEGRAL* spectrometer (SPI), and from the non-contemporaneous observations of the COMPTEL instrument on the Compton Gamma-Ray Observatory *CGRO* and the *Fermi*-GBM. [15–17].

ISGRI is a coded tungsten mask instrument with cadmium-telluride detectors sensitive to photons with energies in the range ~ 15 keV to 1 MeV [18]. SPI is a coded aperture tungsten mask instrument with germanium detectors and a bismuth germanate (BGO) anti-coincidence detector. SPI is sensitive to photons in the range 20 keV to 8 MeV [19]. The COMPTEL instrument [20] was a liquid scintillator/NaI detector sensitive to photons in the energy range 0.75 MeV to 1 MeV. Finally, the *Fermi*-GBM has two detection systems, the first, composed of 12 sodium iodide (NaI) detectors, oriented in different directions, is sensitive to photons <1 MeV whereas the second composed of 2 BGO detectors, is sensitive to photon energies in the range 150 keV − 30 MeV [21]. The flux measurement of [17] is obtained using only the NaI detectors.

We extract UL fluxes from the original spectral energy distributions of [15 and 16], in a conservative manner, as the sum of *CGRO* COMPTEL determinations in range 0.3−1 MeV and adjacent *INTEGRAL* IBIS-ISGRI measurements in the 200-300 keV band. The UL flux obtained from the *Fermi*-GBM is from [17] and is a single pulsed UL in the 0.5-2 MeV band.

IV. SOFT GAMMA RAY BACKGROUND

Magnetars exhibit thermal X-ray emission below 10 keV and a hard pulsed non-thermal X-ray emission with power law tails above 10 keV. This hard X-ray emission can extend to between $150 − 275$ keV [27–29] and appears to turn over above 275 keV due to ULs being obtained with INTEGRAL SPI (20−1000 keV) and CGRO COMPTEL (0.75−30 MeV) [15]. A spectral break above

1 MeV is also inferred by the non-detection of 20 magnetars using *Fermi*-LAT above 100 MeV [30]. The hard X-ray emission is most likely caused by resonant Compton upscattering (RCU) of surface thermal X-rays by non-thermal electrons moving along the magnetic field lines of the magnetosphere. The initial modeling of [31], using B field strengths typical of magnetars, at three times the quantum critical field strength B_c produces flat differential flux spectra with sharp cut-offs at energies directly proportional to the electron Lorentz factor (γ_e) and places the maximum extent of the Compton resonasphere within a few stellar radii of the magnetar surface.

In [32], Monte-Carlo models of the RCU of soft thermal photons, incorporating the relativistic QED resonant cross section, produces flat spectra up to 1 MeV for highly relativistic electrons (γ_e=22), whilst mildly relativistic electrons (γ_e=1.7) demonstrate spectral breaks at 316 keV. In [33], an analytic model of RCU, considering relativistic particle injection (γ_e>>10) and deceleration within magnetic loops predicts a spectral peak at ~ 1 MeV and a narrow annihilation line at 511 keV (both as yet unobserved). This model also places the active field loops emitting photons at $3−10$ stellar radii for a surface B field of $\sim 10^{15}$ G.

The analysis of [31] is recently extended in [34], allowing for a QED Compton cross scattering section which incorporates spin-dependent effects in stronger B fields. Electrons with energies $\lesssim 15$ MeV will emit most energy below 250 keV which is consistent with the hard inferred X-ray turnover above. In [34], the maximum resonant cut-off energy can reach a peak of 810 keV, for γ_e=10 at some magnetar rotational phases and viewing angles which violates COMPTEL ULs, however the model neglects the effects of Compton cooling and attenuation processes such as photon absorption due to magnetic pair creation ($\gamma \to e^+e^-$) and photon splitting ($\perp \to \|\|$). Also, the effect of electron Compton cooling is expected to steepen the cut-offs seen in the predicted hard X-ray spectral tails and allow the models to then be in agreement with the COMPTEL ULs. The emission region is placed at $4 − 15$ and $2.5−30$ stellar radii for γ_e values of 10 and 100 respectively.

The attenuation processes of magnetic pair creation and photon splitting which act to suppress photon emission in RCU are considered in detail in [35] for typical magnetar surface B fields of 10 B_c. In this case, the photon splitting opacity alone constrains the emission region of observed 250 keV emission in magnetars to be outside altitudes of 2-4 stellar radii and photons emitted from the magnetar surface at magnetic co-latitudes <20° can escape with energies >1 MeV for typical magnetar surface B fields of 10 B_c. Also the emission of photons from field loops at <2 stellar radii is suppressed with photon escape energies of no greater then 287 keV. In contrast, emission regions at altitudes of >5 stellar radii guarantee escape of 1 MeV photons at nearly all co-latitudes. The photon opacity caused by pair creation is shown to be much less restrictive and does not impact the <1 MeV band.

Magnetar	Distance kpc	Surface B Field 10^{14} G	Age kyr	UL Flux 300 keV - 1 MeV 10^{10} erg cm^{-2} s^{-1}	UL Luminosity 300 keV - 1 MeV 10^{35} erg s^{-1}
1E 2259+586	$3.2^{+0.2}_{-0.2}$ [22]	0.59	230	1.17 [16]	$1.43^{+0.18}_{-0.17}$
4U 0142+61	$3.6^{+0.4}_{-0.4}$ [23]	1.3	68	8.16 [15]	$12.65^{+2.97}_{-2.66}$
1RXS J170849.0-400910	$3.8^{+0.5}_{-0.5}$ [22]	4.7	9	1.92 [16]	$3.32^{+0.93}_{-0.82}$
1E 1547.0-5408	$4.5^{+0.5}_{-0.5}$ [24]	3.2	0.69	3.20 [17]	$7.75^{+1.82}_{-1.63}$
1E 1841-045	$8.5^{+1.3}_{-1.0}$ [25]	7	4.6	2.56 [16]	$22.13^{+7.28}_{-4.90}$
1E 1048.1-5937	$9.0^{+1.7}_{-1.7}$ [23]	3.9	4.5	3.04 [16]	$29.46^{+12.18}_{-10.07}$

TABLE I Magnetar sample with heliocentric distance in kpc, Surface magnetic field in Gauss, age in kyr, Sum of UL Flux in 300 keV-1 MeV band in erg cm^{-1} s^{-1}, UL luminosity in 300 keV-1 MeV band in erg s^{-1}. UL fluxes and distances are from the references shown, surface B field and age are from the online[48] version of the McGill magnetar catalog [26]. We extract UL fluxes from the original spectral energy distributions of [15 and 16] in a conservative manner as the sum of *CGRO* COMPTEL determinations in range $0.3-1$ MeV and adjacent *INTEGRAL* IBIS-ISGRI measurements in the 200-300 KeV band. The UL flux extracted from [17] is a pulsed UL in the 0.5-2 MeV band obtained from the *Fermi*-GBM.

Finally Fig 8 of reference [35] shows the maximum energies produced by the resonant Compton process alongside the photon escape energies allowed by the photon splitting process (i.e. the maximum photon energies which can escape to an observer) as a function of magnetar rotational phase and obliqueness of rotation (which is the misalignment of the magnetic and rotational axis) and observer angle. It shows that photon emission >1 MeV is permitted at some but not all rotational phases in the meridional case and that in most cases the RCU emission will vary with rotational phase in the 300 keV $-$ 1 MeV band.

Therefore, the RCU process *may* produce a background to the signal we wish to measure and this background might be expected to produce pulsed emission when photon opacity due to photon splitting is taken into account. On the other hand, a spectral turn over is possible if the electrons in the magnetosphere field loops are mildly relativistic. In addition, pulsed emission in magnetars has not been observed in the 300 keV $-$ 1 MeV band which would be suggestive of an RCU emission mechanism. We also note that photon splitting / pair creation opacity will not attenuate photon emission <1 MeV at >10 stellar radii [35]. As axion to photon conversion will occur at $\sim$ 300 stellar radii, photon opacity processes can be disregarded. In addition, the 440 magnetar bursts observed with the *Fermi*-GBM over 5 years have been spectrally soft with typically no emission above 200 keV[36].

A reasonable assumption resulting from the above discussion would be that there is no RCU background and that all emission in the 300 keV $-$ 1 MeV band results from ALP to photon conversion. We instead opt for a slightly more conservative approach and require that any emission from ALP-photon conversion be *bounded* by the observed emission. This results in ULs on the ALP-photon coupling.

V. MAGNETAR CORE TEMPERATURE

We now summarise the need for a magnetar heating mechanism over and above that found in conventional pulsars and discuss temperature modelling which supports the range of values we have chosen for the magnetar core temperature (T_c).

The quiescent X-ray luminosity of magnetars of $10^{34}-10^{35}$ erg s^{-1} exceeds the spin down luminosity of $10^{32}-10^{34}$ erg s^{-1}, thus excluding rotation spin down as the sole magnetar energy source. Furthermore, the lack of Doppler modulation in X-ray pulses arising from magnetars indicates a lack of binary companions, which combined with the slow periods of magnetars ($2-12$ s) excludes an accretion powered interpretation [38 and 39].

In reference [40], the authors show the need for heating by theoretical cooling curves for neutron stars of mass 1.4 $M_\odot$, with and without proton superfluidity in the core, which yield effective surface temperatures below those observed in seven magnetars (including four in our selection, namely: 1E 1841-045, 1RXS J170849.0-400910, 4U 0142+61 and 1E 2259+586). They then use a general relativistic cooling code which accounts for thermal losses from neutrino and photon emission and allows for thermal conduction to show that magnetars are hot inside with $T_c=10^{8.4}$ K at age 1000 yr and temperatures of $10^{9.1}$ K in the crust, where the heat source should be located for efficient warming of the surface, to offset neutrino heat losses from the core.

The authors of [41] consider the case of magnetars born with initial periods of ≤ 3 ms combined with a strong internal toroidal B field of $\geq 3 \times 10^{16}$ G and an exterior dipole B field of $\leq 2 \times 10^{14}$ G. In this case, efficient heating of the core can occur via ambipolar diffusion which has a time varying decay scale as a function of T_c and B field strength. As the core cools, an equilibrium is established between increasing B field decay and reducing neutrino emission, leading to reduced cooling which can keep T_c at $10^{8.9}$ K 2250 yr after magnetar creation.

The magnetar temperature modeling of [42] considers heating throughout the magnetar core arising from magnetic field decay and ambipolar diffusion, together with the cooling caused by the neutrino emission of the modified URCA process and Cooper pairing of nucleons. In this case, the authors find that strong core heating cannot account for the observed surface temperatures and conclude that, as in the case of [40], high surface temperatures require heating of the crust, rather than the
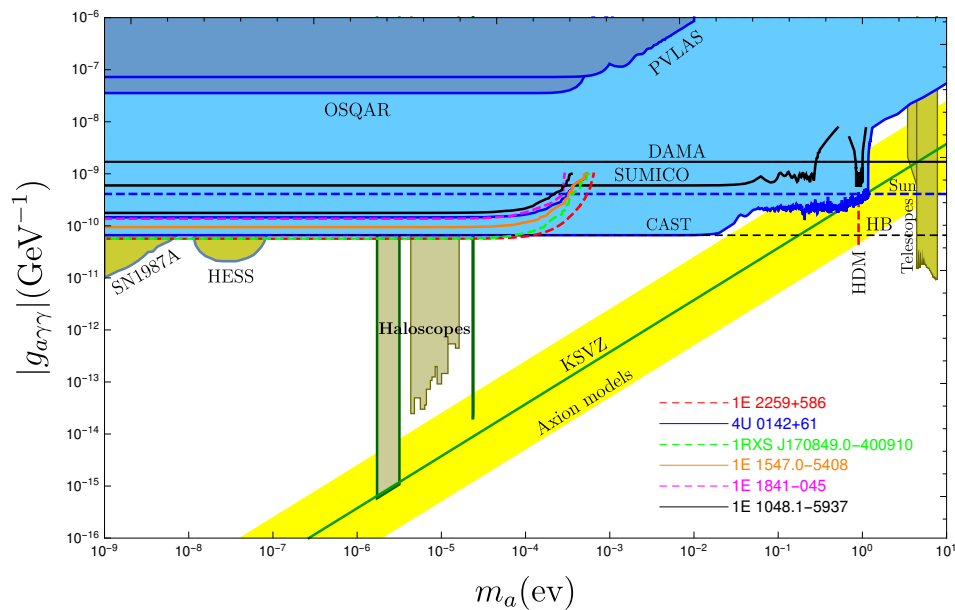
FIG. 1 The constraints on the ALP-photon coupling $g_{a\gamma\gamma}$ for the six magnetars in our sample. The constraints are obtained for emissions in the energy range 300 keV - 1 MeV. The core temperature is assumed to be 10^9 K. The ALP-nucleon coupling g_{aN} is assumed to be such that the ALP luminosity is just sub-dominant to neutrino luminosity at a given temperature. All other constraints are taken from Fig. 6 of [37].

core, with the crust and the core being thermally decoupled from one another. However the authors of [42] show that T_c at 10^4 yr can vary between 0.8×10^8 K with **no** heating of the superfluid core, 1.4×10^8 K with heating of the crust and 5×10^8 K with core heating. At 10^3 yr, with heating of the superfluid core, T_c can reach 7×10^8 K.

The strong B field of magnetars can produce strongly anisotropic thermal conductivity in the neutron star crust whilst also allowing the synchrotron neutrino process to become a predominant cooling mechanism while other contributions to the neutrino emissivity are far more weakly suppressed. These effects allow the temperature at the base of the crust heat blanketing envelope to reach $10^{9.6}$ K while the surface temperature remains at 10^5 and $10^{6.7}$ K [43], for a B field parallel and radial to the neutron star surface respectively. This is compatible with the observed surface temperatures of $10^{6.5} - 10^{6.95}$ K for the seven magnetars in [40] and could allow T_c to exceed 10^9 K.

Finally, the quiescent luminosity of magnetars $10^{34} - 10^{35}$ erg s^{-1} implies a T_c of $(2.7 - \geq 8.0) \times 10^8$ K for a magnetar with an accreted iron envelope and $(1.0 - 5.5) \times 10^8$ K for an accreted light element envelope [44].

There are no published T_c values for the magnetars in our selection. We therefore study the dependence of our results on a range of core temperatures.
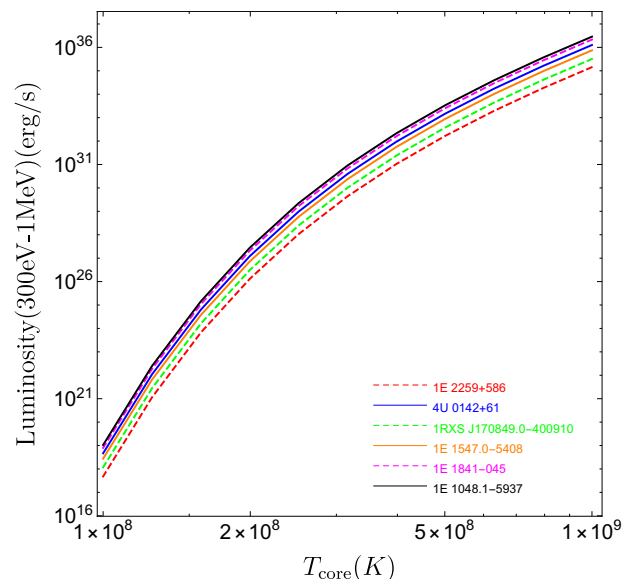

FIG. 2 The luminosity as a function of the core temperature for the different magnetars in our study. The ALP mass is fixed at 10^{-7} eV and the ALP-photon coupling for each magnetar is fixed at the value given in Table II.

VI. RESULTS

The luminosity resulting from ALP-photon conversion in the energy range 300 keV - 1 MeV for the magnetars in Table I is calculated from Eq. A3. The constraints on $g_{a\gamma\gamma}$ for $T_c = 10^9$ K are shown in Figure 1. We see that for magnetars 1RXS J170849.0-400910 and 1E 2259+586, the limits on the ALP-photon coupling coming from conversions rival the current CAST limits for

masses $m_a \lesssim 10^{-4}$ eV.

The ULs on the ALP-photon coupling $g_{a\gamma\gamma}$ for the different magnetars in our sample are shown in Table II. For 1RXS J170849.0-400910 and 1E 2259+586, the ULs on $g_{a\gamma\gamma}$ are 5.69×10^{-11} GeV^{-1} and 5.68×10^{-11} GeV^{-1}, respectively. For the other magnetars in our sample, the ULs are weaker, but still almost competitive with CAST limits.

The constraints become weak and taper off for $m_a \gtrsim 10^{-4}$ eV. This can be understood from the fact that the ALP-photon mixing angle becomes small for large ALP masses and the probability of conversion becomes highly reduced.

Magnetar	$g_{a\gamma\gamma}$ (GeV^{-1})
1E 2259+586	5.68×10^{-11}
4U 0142+61	1.47×10^{-10}
1RXS J170849.0-400910	5.69×10^{-11}
1E 1547.0-5408	9.43×10^{-11}
1E 1841-045	1.37×10^{-10}
1E 1048.1-5937	1.77×10^{-10}

TABLE II Results: The upper limit on the ALP-photon coupling $g_{a\gamma\gamma}$ obtained from conversions for the different magnetars in our sample. The ALP mass is chosen to be 10^{-7} eV for all benchmarks shown in this table. The ALP-nucleon coupling is taken to be such that the ALP luminosity is just sub-dominant to the neutrino luminosity at a given temperature. The core temperature is taken to be 10^9 K.

The luminosity as a function of the core temperature T_c is studied in Fig. 2. The ALP mass is fixed at 10^{-7} eV and the ALP-photon coupling for each magnetar is fixed at the value given in Table II. We can see that there is a steep reduction in the luminosity with decreasing core temperature. This can be understood from the temperature dependence of the nucleon bremsstrahlung process as well as the normalized ALP spectrum.

In Fig. 3, the constraints on the ALP-photon coupling $g_{a\gamma\gamma}$ are shown as a function of the core temperature. The ALP mass is fixed at 10^{-7} eV and the luminosity from ALP-photon conversion is assumed to saturate the UL luminosity listed in Table I for each magnetar. As the core temperature is reduced, the ALP production from the core drops appreciably and to saturate the UL on the luminosity, the probability of conversion (and hence $g_{a\gamma\gamma}$) must show a corresponding increase. For 1E 2259+586, the core temperature at which the constraint on $g_{a\gamma\gamma}$ coincides with CAST is 9.63×10^8 K. For 1RXS J170849.0-400910, the corresponding value is 9.66×10^8 K.

VII. DISCUSSION: PROPOSED MAGNETAR OBSERVATIONS WITH THE GBM

The GBM is a non-imaging instrument with a wide field of view. However, it is possible to assign detected events to pulsar point sources using the Earth Occultation Technique (EOT) or pulsar timing models. EOT uses a predefined catalogue of sources which exhibit step like changes in photon count rate as seen by the GBM, when the sources are eclipsed by or rise above the Earth
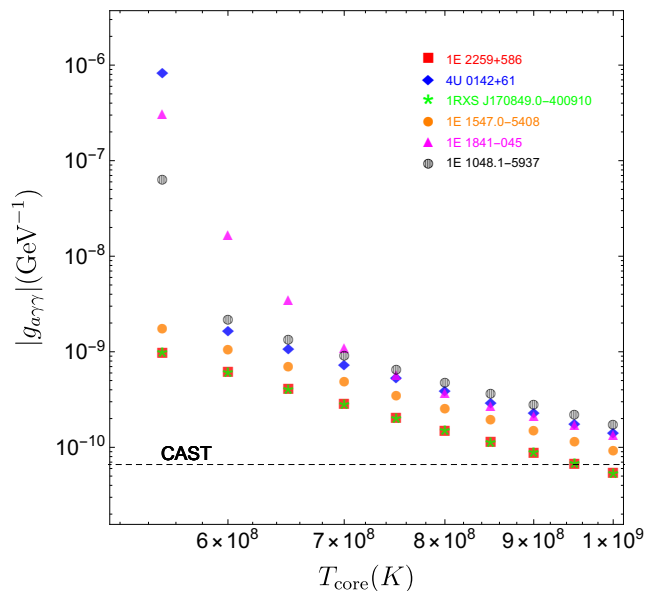

FIG. 3   The UL on the ALP-photon coupling $g_{a\gamma\gamma}$ as the core temperature is varied, for the different magnetars in our study. The ALP mass is fixed at 10^{-7} eV and the luminosity from ALP-photon conversion is assumed to saturate UL luminosity listed in Table I for each magnetar. The horizontal dashed line shows the current CAST limits. For 1E 2259+586, the core temperature at which the constraint on $g_{a\gamma\gamma}$ beats CAST is 9.63×10^8 K. For 1RXS J170849.0-400910, the corresponding value is 9.66×10^8 K.

limb. Initially, 209 sources have been monitored using 3 years of data with 9 sources detected in the 100-300 keV energy band [45].

The 53 day orbital precession period of *Fermi* can also be used to apply EOT without the use of a predefined source catalogue. Using the Imaging with a Differential Filter using the Earth Occultation Method (IDEOM), the Earth limb is projected onto the sky and used to determine count rates from 600, 000 virtual sources with a 0.25° spacing [46], identifying 17 new sources.

The *Fermi*-GBM Occultation project currently monitors 248 sources in the energy range 8 keV $-$ 1 MeV with the majority of the signal being in 12-50 keV band[47].

In contrast, the author of [17] uses a pulsar timing method rather than an occultation technique. The CTIME data of the GBM is used to provide photon counts for 4 magnetars, 1RXS J170849.0-400910, 1E 1841-045, 4U 0142+61 and 1E 1547.0-5408, obtained with all 12 NaI detectors. The photon counts are attributed to the peak pulsed emission of each magnetar by epoch folding and the use of timing models (obtained with the Rossi X-ray Timing Explorer), which allow each event to be tagged by pulsar phase. This count rate is converted to an energy flux for 7 energy channels between 11 keV $-$ 2 MeV by determining the GBM effective area as a function of photon direction, energy and probability of detection of a photon with a given energy. This yields pulsed ULs, just a factor of a few above those obtained by COMPTEL for J170849.0-400910, 1E 1841-045 and 4U 0142+6.

The GBM is thus a very useful instrument to determine the UL soft gamma-ray fluxes of the 23 confirmed magnetars[48] as listed in the McGill Magnetar Catalog [26], most of which have no ULs defined in the 300 keV − 1 MeV band of interest in axion conversion.

VIII. CONCLUSIONS

In this paper, we have explored constraints on the ALP-photon coupling resulting from the conversion of ALPs into photons in the magnetosphere of magnetars. The basic mechanism is as follows: relativistic ALPs emitted from the core by nucleon bremsstrahlung escape into the magnetosphere, where they convert to photons in the presence of the neutron star magnetic field. We have studied the resulting ALP-induced quiescent soft-gamma flux (300 keV - 1 MeV) in a selection of 6 magnetars, for which there exists published ULs from *CGRO* COMPTEL, *INTEGRAL* SPI/IBIS/ISGRI and the *Fermi*-GBM. The probability of conversion has been calculated from the ALP-photon propagation equations, after properly calculating the photon refractive index in the quantum critical magnetic field.

We discussed the possible astrophysical background in the 300 keV − 1 MeV band and argued that contributions from RCU should be suppressed. A reasonable assumption could be that the observed emission in that band is from ALP-photon conversions; however, we opt for the more conservative requirement that the emission from ALP-photon conversion be bounded by the observed emission. This results in ULs on the ALP-photon coupling depicted in Figure 1. For a core temperature of 10^9 K, the constraints on the ALP-photon coupling coming from magnetars 1E 2259+586 and J170849.0-400910 are stronger than the limits obtained from the CAST experiment.

When interpreting our results in Figure 1, the following caveats should be kept in mind:

(i) The luminosity of ALPs produced from the core depends on the ALP-nucleon coupling g_{aN}, which has been taken so that the ALP luminosity is just sub-dominant to the neutrino luminosity at a given temperature.

(ii) Since the magnetars in our selection have no published values of T_c, we have studied the dependence of our results on a range of core temperatures. This is shown in Figure 2 and Figure 3. It is clear that for core temperatures lower than $\sim 9.6 \times 10^8$ K, our constraints become weaker than the CAST limits.

Our results motivate a program of studying quiescent soft gamma ray emission from magnetars in the 300 keV - 1 MeV band by the *Fermi*-GBM Collaboration. The GBM will be able to determine the UL soft gamma-ray fluxes of confirmed magnetars, most of which have no ULs defined in the 300 keV − 1 MeV band. With these ULs, it is possible that even more stringent constraints on the ALP-photon coupling may be obtained, comparable or beating CAST bounds for even lower core temperatures.

Appendix A: Predicted ALP-photon Luminosity

In this Appendix, we outline our calculation of the predicted photon luminosity coming from ALP-photon conversions. We denote the ALP spectrum from nucleon-nucleon bremsstrahlung production in the core by $dN_a/d\omega$ and normalize it by requiring $\int_0^\infty d\omega\, dN_a/d\omega = 1$. For the energy range $\omega \subset (\omega_i, \omega_f)$, the luminosity is

$$L_{a\to\gamma} = \frac{N_a}{2\pi} \int_0^{2\pi} d\theta \int_{\omega_i}^{\omega_f} d\omega\, \omega \frac{dN_a}{d\omega} P_{a\to\gamma}(\omega,\theta)\,. \tag{A1}$$

The number of ALPs emitted by the magnetar, N_a, can be bounded by requiring that ALPs are a subdominant source of cooling compared to neutrinos:

$$L_a = N_a \int_0^\infty d\omega\, \omega \frac{dN_a}{d\omega} \leq L_\nu = 4\pi \int_0^{r_0} dr\, r^2 \dot{q}_\nu, \tag{A2}$$

with $\dot{q}_\nu$ denoting the neutrino emissivity. Integrating the uniform emissivity over the magnetar volume, we obtain

$$N_a \leq \frac{4\pi r_0^3 \dot{q}_\nu}{3 \int_0^\infty d\omega\, \omega \frac{dN_a}{d\omega}},$$

Then, the final expression for the luminosity is

$$L_{a\to\gamma} = \frac{4\pi r_0^3 \dot{q}_\nu}{3 \int_0^\infty d\omega\, \omega \frac{dN_a}{d\omega}} \int_0^{2\pi} d\theta \int_{\omega_i}^{\omega_f} d\omega\, \omega \frac{dN_a}{d\omega} P_{a\to\gamma}(\omega,\pi/2). \tag{A3}$$

This is our master equation, used to set limits on the ALP-photon coupling. We describe the different ingredients that appear in the master equation:

(i) For the normalized ALP spectrum, we use

$$\frac{dN_a}{d\omega} = \frac{x^2(x^2 + 4\pi^2)e^{-x}}{8(\pi^2\zeta_3 + 3\zeta_5)(1 - e^{-x})}, \tag{A4}$$

where $x = \omega/k_B T$. This corresponds to ALP production by nucleon bremsstrahlung emission in the degenerate limit [9 and 50].

(ii) For the neutrino emissivity, we use the case where modified URCA processes are the dominant production mode for neutrinos in the core [44 and 51],

$$\dot{q}_\nu = (7 \times 10^{20}\, \text{erg} \cdot \text{s}^{-1} \cdot \text{cm}^{-3}) \left(\frac{\rho}{\rho_0}\right)^{2/3} R_M \left(\frac{T}{10^9\, \text{K}}\right)^8, \tag{A5}$$

with ρ being the magnetar density and $\rho_0 = 2.8 \times 10^{14}\, \text{g} \cdot \text{cm}^{-3}$ the nuclear saturation density. The onset of proton or neutron superfluidity is parametrized by a suppression factor $R_M \leq 1$.

(iii) The probability of conversion $P_{a\to\gamma}$ is obtained by numerically solving the propagation equations Eq. 2. For the calculations, we need the refractive indices that appear in Eq. 3. These refractive indices are derived in Appendix B.

Appendix B: Calculation of Refractive Indices

In this Appendix, we provide general expressions for the photon refractive indices in the parallel and perpendicular directions. We are interested in several different regimes of the photon frequency and the strength of the external magnetic field:

(i) $\omega \ll 2m_e$ and $B \ll B_c$: soft X-rays in an external magnetic field that is much weaker than the critical strength. This regime is relevant for the conversion of less energetic ALPs into photons at the radius of conversion $\sim 500 r_0$, where $B \sim 10^{-5} B_c$. Since the photon energies are much smaller than m_e, the Euler-Heisenberg approximation can be used to calculate the refractive indices.

(ii) $\omega \lesssim 2m_e$ and $B \ll B_c$, with $\left(\frac{\omega}{2m_e}\right)^2 \left(\frac{B}{B_c}\right)^2 \ll 1$: hard X-rays and soft gamma-rays in an external magnetic field that is much weaker than the critical strength. This regime is relevant for the conversion of energetic ALPs with $\omega \sim \mathcal{O}(100)$ keV - $\mathcal{O}(1)$ MeV into photons at the radius of conversion $\sim 500 r_0$, where $B \sim 10^{-5} B_c$. This regime is relevant for the observational signatures considered in this paper.

(iii) $\omega \lesssim 2m_e$ and $B > B_c$: hard X-rays and soft gamma-rays in an external magnetic field that is stronger than the critical strength. This regime is relevant for the conversion of energetic ALPs with $\omega \sim \mathcal{O}(100)$ keV - $\mathcal{O}(1)$ MeV into photons from the magnetar surface to a distance of $\sim 3 r_0$.

We now turn to a discussion of the refractive indices in regimes (ii) and (iii), which are relevant for this paper.

Quantum corrections to the photon propagator can be studied using the photon polarization tensor $\Pi^{\mu\nu}$, defined in the following way [52]

$$\mathcal{L} \supset -\frac{1}{2} \int_{x'} A_\mu(x) \Pi^{\mu\nu}(x, x') A_\nu(x') \,, \tag{B1}$$

where A_μ is the propagating photon. To evaluate $\Pi^{\mu\nu}$, we can consider the perpendicular and parallel components of the momentum four-vector k^μ. We note that these components are defined with respect to the external magnetic field $\vec{B}$, which we take to point in the direction $\vec{e}_1$: $k^\mu = k_\parallel^\mu + k_\perp^\mu$, $k_\parallel^\mu = (\omega, k^1, 0, 0)$, and $k_\perp^\mu = (0, 0, k^2, k^3)$. The metric tensor can likewise be decomposed into the parallel and perpendicular directions: $g^{\mu\nu} = g_\parallel^{\mu\nu} + g_\perp^{\mu\nu}$, where $g_\parallel^{\mu\nu} = \mathrm{diag}(-1, +1, 0, 0)$ and $g_\perp^{\mu\nu} = \mathrm{diag}(0, 0, +1, +1)$.

We will assume a pure and homogeneous external magnetic field to work out the photon polarization tensor, since taking into account the spatial variation of the magnetic field would be significantly more complicated. This is justified, since the dipolar magnetic field varies at a scale given by the magnetar radius, while the photon wavelength is much smaller in the soft gamma-ray regime. At one loop, the polarization tensor is given by [53–56],

$$\Pi^{\mu\nu}(k) = \frac{\alpha}{2\pi} \int_{-1}^1 \frac{d\nu}{2} \int_0^{\infty - i\eta} \frac{ds}{s} \left\{ e^{-i\Phi_0 s} \left[-N_0 k^\mu k^\nu + (N_1 - N_0) \left(g_\parallel^{\mu\nu} k_\parallel^2 - k_\parallel^\mu k_\parallel^\nu \right) \right. \right.$$
$$\left. \left. + (N_2 - N_0) \left(g_\perp^{\mu\nu} k_\perp^2 - k_\perp^\mu k_\perp^\nu \right) \right] + (1 - \nu^2) e^{-i(m_e^2 - i\epsilon)s} k^\mu k^\nu \right\} \,, \tag{B2}$$

where $\Phi_0 = m_e^2 - i\epsilon + n_1 k_\parallel^2 + n_2 k_\perp^2$, s is the proper time, ν governs the loop momentum distribution, and ϵ and η are parameters that tend to 0^+. The external magnetic field appears in the scalar functions N_0, N_1, N_2, n_1 and n_2. In terms of the variable $z = eBs$, these functions are given by

$$N_0(z) = \frac{z}{\sin z} (\cos \nu z - \nu \sin \nu z \cot z) \,, \qquad\qquad n_1(z) = \frac{1 - \nu^2}{4} \,,$$

$$N_1(z) = z(1 - \nu^2) \cot z \,, \qquad\qquad n_2(z) = \frac{\cos \nu z - \cos z}{2z \sin z} \,,$$

$$N_2(z) = \frac{2z (\cos \nu z - \cos z)}{\sin^3 z} \,. \tag{B3}$$

The polarization tensor is most compactly expressed in terms of the projection operators $P_\parallel^{\mu\nu}$ and $P_\perp^{\mu\nu}$, defined in the following way

$$P_\parallel^{\mu\nu} = g_\parallel^{\mu\nu} - \frac{k_\parallel^\mu k_\parallel^\nu}{k_\parallel^2} \qquad \text{and} \qquad P_\perp^{\mu\nu} = g_\perp^{\mu\nu} - \frac{k_\perp^\mu k_\perp^\nu}{k_\perp^2} \,, \tag{B4}$$

in terms of which the tensor can be re-expressed as [53]

$$\Pi^{\mu\nu}(k) = P_\parallel^{\mu\nu} \Pi_\parallel + P_\perp^{\mu\nu} \Pi_\perp \,, \tag{B5}$$

where

$$\left\{ \begin{matrix} \Pi_\parallel \\ \Pi_\perp \end{matrix} \right\} = \frac{\alpha}{2\pi} \int_{-1}^1 \frac{d\nu}{2} \int_0^{\infty - i\eta} \frac{ds}{s} \left[e^{-i\Phi_0 s} \left\{ \begin{matrix} k_\parallel^2 N_1 + k_\perp^2 N_0 \\ k_\parallel^2 N_0 + k_\perp^2 N_2 \end{matrix} \right\} \right] \,. \tag{B6}$$

The expression in Eq. B6 is amenable to a perturbative expansion, which we now explore.

1. $\omega \lesssim 2m_e$ and $B \ll B_c$, with $\left(\frac{\omega}{2m_e}\right)^2 \left(\frac{B}{B_c}\right)^2 \ll 1$

We first note that a perturbative expansion of Π_p^{pert} (where $p = \parallel, \perp$) in powers of the magnetic field can be obtained by an expansion in powers of $(eB)^{2n}$:

$$\Pi_p^{\mathrm{pert}} = \sum_{n=0}^{\infty} \Pi_p^{(2n)} \,, \tag{B7}$$

with the even powers being due to Furry's theorem, and

$$\Pi_p^{(2n)} = \frac{(eB)^{2n}}{n!} \left[\left(\frac{\partial}{\partial(eB)^2} \right)^n \Pi_p \right]_{eB=0} \,, \tag{B8}$$

Since the limit $z \to 0$ does not admit any poles in the complex s plane for the integrands, the integration over s can be performed on the real positive axis. This yields the following expressions for the $\Pi_p^{(2n)}$ [57]:

$$\left\{ \begin{matrix} \Pi_\parallel^{(2n)} \\ \Pi_\perp^{(2n)} \end{matrix} \right\} = \frac{\alpha}{2\pi} \int_{-1}^{1} \frac{d\nu}{2} \int_0^\infty \frac{ds}{s} \, e^{-i\phi_0 s} \frac{z^{2n}}{n!} \left[\left(\frac{\partial}{\partial z^2} \right)^n \left(\left\{ \begin{matrix} k_\parallel^2 N_1 + k_\perp^2 N_0 \\ k_\parallel^2 N_0 + k_\perp^2 N_2 \end{matrix} \right\} e^{-isk_\perp^2 \tilde{n}_2} \right) \right]_{z=0}, \quad \text{(B9)}$$

where $\tilde{n}_2 = n_2 - \frac{1-\nu^2}{4} = \mathcal{O}(z^2)$.

The integral over s in Eq. B9 can be performed explicitly. Using the expressions in Eq. B3, one obtains

$$\Pi_p^{(2n)} = \frac{\alpha}{2\pi} \int_{-1}^{1} \frac{d\nu}{2} \sum_{l=0}^{n-1} \frac{(2n+l-1)!}{(-1)^{n+l}} \left[k_\parallel^2 c_p^{\parallel (n,l)}(\nu^2) + k_\perp^2 c_p^{\perp (n,l)}(\nu^2) \right] \left(\frac{eB}{m_e^2} \right)^{2n} \left(\frac{k_\perp^2}{m_e^2} \right)^l, \quad \text{(B10)}$$

where the coefficients $c_p^{\parallel (n,l)}(\nu^2)$ and $c_p^{\perp (n,l)}(\nu^2)$ can be obtained explicitly from expanding Eq. B3.

We note that a perturbative expansion can be obtained when both expansion parameters in Eq. B10 are small:

$$\frac{eB}{m_e^2} \equiv \frac{B}{B_c} \ll 1 \qquad \text{and} \qquad \left(\frac{B}{B_c} \right)^2 \frac{\omega^2 \sin^2 \theta}{m_e^2} \ll 1, \quad \text{(B11)}$$

where we have introduced the angle θ between the magnetic field and the photon propagation direction. The leading order tensor is

$$\left\{ \begin{matrix} \Pi_\parallel^{(2)} \\ \Pi_\perp^{(2)} \end{matrix} \right\} = -\frac{\alpha}{12\pi} \int_{-1}^{1} \frac{d\nu}{2} \left(\frac{eB}{\phi_0} \right)^2 (1-\nu^2)^2 \left[\left\{ \begin{matrix} \frac{-2}{1-\nu^2} \\ 1 \end{matrix} \right\} k_\parallel^2 + \left\{ \begin{matrix} 1 \\ \frac{5-\nu^2}{2(1-\nu^2)} \end{matrix} \right\} k_\perp^2 \right]. \quad \text{(B12)}$$

The integration over ν finally yields [58 and 59]

$$\left\{ \begin{matrix} \Pi_\parallel^{(2)} \\ \Pi_\perp^{(2)} \end{matrix} \right\} = -\frac{\alpha}{2\pi} \left(\frac{B}{B_c} \right)^2 \omega^2 \sin^2 \theta \frac{2}{45} \left\{ \begin{matrix} 7 \\ 4 \end{matrix} \right\}, \quad \text{(B13)}$$

The corresponding indices of refraction are given by $n_p = 1 - \frac{1}{2\omega^2} \Re(\Pi_p)$, which yields

$$\left\{ \begin{matrix} n_\parallel \\ n_\perp \end{matrix} \right\} = 1 + \frac{\alpha}{4\pi} \left(\frac{B}{B_c} \right)^2 \sin^2 \theta \frac{2}{45} \left\{ \begin{matrix} 7 \\ 4 \end{matrix} \right\} + \mathcal{O}\left((eB)^4 \right). \quad \text{(B14)}$$

2. $\omega \lesssim 2m_e$ and $B > B_c$

This regime is relevant for the conversion of energetic ALPs with $\omega \sim \mathcal{O}(100)$ keV - $\mathcal{O}(1)$ MeV into photons from the magnetar surface to a distance of $\sim 3r_0$. We only quote the final answer here, referring to [60] for a full derivation:

$$\left\{ \begin{matrix} n_\parallel \\ n_\perp \end{matrix} \right\} = 1 + \frac{\alpha}{4\pi} \sin^2 \theta \left[\left(\frac{2}{3} \frac{B}{B_c} - \Sigma \right) \left\{ \begin{matrix} 1 \\ 0 \end{matrix} \right\} - \left[\frac{2}{3} + \frac{B_c}{B} \ln \left(\frac{B_c}{B} \right) \right] \left\{ \begin{matrix} 1 \\ -1 \end{matrix} \right\} + \mathcal{O}\left(\frac{1}{eB} \right) + \mathcal{O}(\omega^2) \right]. \quad \text{(B15)}$$

Here, $\Sigma \sim \mathcal{O}(1)$ is a constant.

---

a) Electronic mail: sheridan.j.lloyd@durham.ac.uk
b) Electronic mail: p.m.chadwick@durham.ac.uk
c) Electronic mail: anthony.brown@durham.ac.uk
d) Electronic mail: ghk@ou.edu
e) Electronic mail: kuver.sinha@ou.edu

[1] R. D. Peccei and H. R. Quinn, Phys. Rev. Lett. **38**, 1440 (1977), [,328(1977)].
[2] S. Weinberg, Phys. Rev. Lett. **40**, 223 (1978).
[3] M. Dine, W. Fischler, and M. Srednicki, Phys. Lett. **104B**, 199 (1981).
[4] P. W. Graham, I. G. Irastorza, S. K. Lamoreaux, A. Lindner, and K. A. van Bibber, Ann. Rev. Nucl. Part. Sci. **65**, 485 (2015), arXiv:1602.00039 [hep-ex].
[5] J.-F. Fortin and K. Sinha, JHEP **06**, 048 (2018), arXiv:1804.01992 [hep-ph].
[6] J.-F. Fortin and K. Sinha, JHEP **01**, 163 (2019), arXiv:1807.10773 [hep-ph].
[7] S. J. Lloyd, P. M. Chadwick, and A. M. Brown, Phys. Rev. **D100**, 063005 (2019), arXiv:1908.03413 [astro-ph.HE].
[8] The conversion of relativistic ALPs near neutron stars has a long history, starting with the work of Morris [61] where the probability of conversion was overestimated, followed by the classic paper by Raffelt and Stodolsky [14] who correctly accounted for non-linear QED and the photon mass in the ALP-photon conversion equations. Raffelt and Stodolsky performed an order of magnitude calculation of the conversion probability near the magnetar surface and concluded that it was too small to lead to observable signals (the photon mass term dominates over the ALP-photon mixing term at the surface). However, the conversion does in fact become appreciable away from the surface, due to the different scaling of the photon mass ($\sim 1/r^6$) compared to the ALP-photon mixing ($\sim 1/r^3$).

[9] N. Iwamoto, Phys. Rev. Lett. **53**, 1198 (1984).

[10] R. P. Brinkmann and M. S. Turner, Phys. Rev. **D38**, 2338 (1988).

[11] In the soft-gamma ray regime, one has to start directly from the photon polarization tensor and take appropriate limits, instead of starting with the Euler-Heisenberg Lagrangian.

[12] A. Sedrakian, Phys. Rev. **D93**, 065044 (2016), arXiv:1512.07828 [astro-ph.HE].

[13] B. Berenji, J. Gaskins, and M. Meyer, Phys. Rev. **D93**, 045019 (2016), arXiv:1602.00091 [astro-ph.HE].

[14] G. Raffelt and L. Stodolsky, Phys. Rev. **D37**, 1237 (1988).

[15] P. R. d. Hartog, L. Kuiper, W. Hermsen, V. M. Kaspi, R. Dib, J. Knoedlseder, and F. P. Gavriil, Astron. Astrophys. **489**, 245 (2008), arXiv:0804.1640 [astro-ph].

[16] L. Kuiper, W. Hermsen, P. R. d. Hartog, and W. Collmar, Astrophys. J. **645**, 556 (2006), arXiv:astro-ph/0603467 [astro-ph].

[17] F. ter Beek, *FERMI GBM detections of four AXPs at soft gamma-rays*, Thesis (2012).

[18] F. Lebrun *et al.*, Astron. Astrophys. **411**, L141 (2003), arXiv:astro-ph/0310362 [astro-ph].

[19] G. Vedrenne *et al.*, Astronomy and Astrophysics **411**, L63 (2003).

[20] V. Schoenfelder *et al.*, Astrophysical Journal Supplement Series **86**, 657 (1993).

[21] C. Meegan *et al.*, Astrophys. J. **702**, 791 (2009), arXiv:0908.0450 [astro-ph.IM].

[22] R. Kothes and T. Foster, Astrophys. J. **746**, L4 (2012).

[23] M. Durant and M. H. van Kerkwijk, Astrophys. J. **650**, 1070 (2006), arXiv:astro-ph/0606027 [astro-ph].

[24] A. Tiengo *et al.*, Astrophys. J. **710**, 227 (2010), arXiv:0911.3064 [astro-ph.HE].

[25] D. A. Leahy and W. Tian, Astrophys. J. **677**, 292 (2008), arXiv:0709.4667 [astro-ph].

[26] S. A. Olausen and V. M. Kaspi, Astrophys. J. Suppl. **212**, 6 (2014), arXiv:1309.4167 [astro-ph.HE].

[27] L. Kuiper, W. Hermsen, and M. Mendez, Astrophys. J. **613**, 1173 (2004), arXiv:astro-ph/0404582 [astro-ph].

[28] D. Gotz, S. Mereghetti, A. Tiengo, and P. Esposito, Astron. Astrophys. **449**, L31 (2006), arXiv:astro-ph/0602359 [astro-ph].

[29] P. R. d. Hartog, L. Kuiper, and W. Hermsen, Astron. Astrophys. **489**, 263 (2008), arXiv:0804.1641 [astro-ph].

[30] J. Li, N. Rea, D. F. Torres, and E. de Ona-Wilhelmi, Astrophys. J. **835**, 30 (2017), arXiv:1607.03778 [astro-ph.HE].

[31] M. G. Baring and A. K. Harding, *Conference on Isolated Neutron Stars: From the Interior to the Surface London, England, April 24-28, 2006*, Astrophys. Space Sci. **308**, 109 (2007), arXiv:astro-ph/0610382 [astro-ph].

[32] S. Zane, R. Turolla, L. Nobili, and N. Rea, Adv. Space Res. **47**, 1298 (2011), arXiv:1008.1537 [astro-ph.HE].

[33] A. M. Beloborodov, Astrophys. J. **762**, 13 (2013), arXiv:1201.0664 [astro-ph.HE].

[34] Z. Wadiasingh, M. G. Baring, P. L. Gonthier, and A. K. Harding, Astrophys. J. **854**, 98 (2018), arXiv:1712.09643 [astro-ph.HE].

[35] K. Hu, M. G. Baring, Z. Wadiasingh, and A. K. Harding, Mon. Not. Roy. Astron. Soc. **486**, 3327 (2019), arXiv:1904.03315 [astro-ph.HE].

[36] A. C. Collazzi *et al.*, Astrophys. J. Suppl. **218**, 11 (2015), arXiv:1503.04152 [astro-ph.HE].

[37] V. Anastassopoulos *et al.* (CAST), Nature Phys. **13**, 584 (2017), arXiv:1705.02290 [hep-ex].

[38] T. Enoto, S. Kisaka, and S. Shibata, Rept. Prog. Phys. **82**, 106901 (2019).

[39] V. M. Kaspi and A. Beloborodov, Ann. Rev. Astron. Astrophys. **55**, 261 (2017), arXiv:1703.00068 [astro-ph.HE].

[40] A. D. Kaminker, D. G. Yakovlev, A. Y. Potekhin, N. Shibazaki, P. S. Shternin, and O. Y. Gnedin, Mon. Not. Roy. Astron. Soc. **371**, 477 (2006), arXiv:astro-ph/0605449 [astro-ph].

[41] S. Dall'Osso, S. N. Shore, and L. Stella, Mon. Not. Roy. Astron. Soc. **398**, 1869 (2009), arXiv:0811.4311 [astro-ph].

[42] W. C. G. Ho, K. Glampedakis, and N. Andersson, Mon. Not. Roy. Astron. Soc. **422**, 2632 (2012), arXiv:1112.1415 [astro-ph.HE].

[43] A. Y. Potekhin, G. Chabrier, and D. G. Yakovlev, *Conference on Isolated Neutron Stars: From the Interior to the Surface London, England, April 24-28, 2006*, Astrophys. Space Sci. **308**, 353 (2007), arXiv:astro-ph/0611014 [astro-ph].

[44] A. M. Beloborodov and X. Li, Astrophys. J. **833**, 261 (2016), arXiv:1605.09077 [astro-ph.HE].

[45] C. A. Wilson-Hodge *et al.*, Astrophys. J. Suppl. **201**, 33 (2012), arXiv:1201.3585 [astro-ph.HE].

[46] J. Rodi, M. L. Cherry, G. L. Case, A. Camero-Arranz, V. Chaplin, M. H. Finger, P. Jenke, and C. A. Wilson-Hodge, Astron. Astrophys. **562**, A7 (2014), arXiv:1304.1478 [astro-ph.HE].

[47] https://gammaray.msfc.nasa.gov/gbm/science/earth_occ.html accessed on 25th November 2019.

[48] http://www.physics.mcgill.ca/~pulsar/magnetar/main.html accessed on 25th November 2019.

[49] J.-F. Fortin, H. Guo, and K. Sinha, Work in progress.

[50] G. G. Raffelt, *Stars as laboratories for fundamental physics* (1996).

[51] B. L. Friman and O. V. Maxwell, Astrophys. J. **232**, 541 (1979).

[52] W. Dittrich and H. Gies, Springer Tracts Mod. Phys. **166**, 1 (2000).

[53] A. E. Shabad, Annals Phys. **90**, 166 (1975).

[54] W.-y. Tsai, Phys. Rev. **D10**, 2699 (1974).

[55] D. B. Melrose and R. J. Stoneham, Nuovo Cim. **A32**, 435 (1976).

[56] L. F. Urrutia, Phys. Rev. **D17**, 1977 (1978).

[57] F. Karbstein, *Proceedings, International Wokshop on Strong Field Problems in Quantum Theory: Tomsk, Russia, June 6-11, 2016*, Russ. Phys. J. **59**, 1761 (2017), arXiv:1607.01546 [hep-ph].

[58] F. Karbstein and R. Shaisultanov, Phys. Rev. **D91**, 085027 (2015), arXiv:1503.00532 [hep-ph].

[59] F. Karbstein, Phys. Rev. **D88**, 085033 (2013), arXiv:1308.6184 [hep-th].

[60] J. S. Heyl and L. Hernquist, J. Phys. **A30**, 6485 (1997), arXiv:hep-ph/9705367 [hep-ph].

[61] D. E. Morris, Phys. Rev. **D34**, 843 (1986).